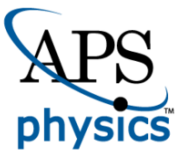

Melting and High P-T Transitions of Hydrogen up to 300 GPa

Chang-sheng Zha, Hanyu Liu, John S. Tse, and Russell J. Hemley

Phys. Rev. Lett. **119**, 075302 — Published 16 August 2017

DOI: 10.1103/PhysRevLett.119.075302

Melting and high *P-T* transitions of hydrogen to 300 GPa

Chang-sheng Zha[1*], Hanyu Liu[1], John S. Tse[2], and Russell J. Hemley[3]

[1]*Geophysical Laboratory, Carnegie Institution of Washington, Washington, DC 20015 USA*

[2]*Department of Physics, University of Saskatchewan, Saskatoon SK, S7N 5B2 Canada*

[3]*Department of Civil and Environmental Engineering, The George Washington University, Washington, DC 20052 USA*

High *P-T* Raman spectra of hydrogen in the vibron and lattice mode regions were measured up to 300 GPa and 900 K using externally heated diamond anvil cell techniques. A new melting line determined from the disappearance of lattice mode excitations was measured directly for the first time above 140 GPa. The results differ from theoretical predictions and extrapolations from lower pressure melting relations. In addition, discontinuities in Raman frequencies are observed as a function of pressure and temperature indicative of phase transition at these conditions. The appearance of a new Raman feature near 2700 cm^{-1} at ~300 GPa and 370 K indicates the transformation to a new crystalline phase. Theoretical calculations of the spectrum suggest the new phase is the proposed *Cmca*-4 metallic phase. The transition pressure is close to that of a recently reported transition observed on dynamic compression.

[*]Author to whom correspondence should be addressed. Electronic mail: czha@carnegiescience.edu

The predicted molecular to atomic and related insulator to metallic transitions in hydrogen at very high pressures remain an important problem in condensed matter physics [1-4], In recent yeas, there has been increasing experimental and theoretical focus on hot dense hydrogen at megabar pressures. A critical question concerns the melting line, which appears to have a temperature maximum near 100 GPa [5-9]. This maximum is broadly consistent with theoretical calculations [10-15]. However, direct measurements of melting above 140 GPa have not been reported. The measurements at higher pressures are important for determining whether hydrogen could have a fluid ground state and exhibit novel quantum superfluid and superconducting predicted at multimegabar pressures calculations [16]. The melting behavior also provides constraints on additional possible transitions in the solid [17-20] and fluid (*e.g.,* plasma phase transition) [12, 21-32] under high *P*-*T* conditions. Indeed, dynamic [21-23] and static [24-26] compression experiments as well as theoretical calculations [12, 27-32] disagree on the nature and conditions of such transitions. Resolution of these issues requires additional high *P*-*T* experiments, including direct measurements of melting at multimegabar (>200 GPa) pressures. We have developed improved external heating techniques for the study of hot dense hydrogen on static compression to multimegabar pressures. We have succeeded in heating hydrogen in previously unexplored *P*-*T* regimes to 300 GPa. The results reveal new *P*-*T* phase transitions, including the suggested existence of a high *P*-*T* metallic phase at the highest pressures.

Resistively heated diamond anvil cell (DAC) techniques played an important role in the early melting measurements on hydrogen at lower pressures. The large refractive index difference between liquid and solid with the large sample sizes used at low to modest pressures facilitate the determination of melting by direct visual observation. With these techniques heating is uniform and the sample temperature can be precisely measured by thermocouples and is repeatable. Using these techniques, the melting line was measured to 373 K and 7.7 GPa and fit to the Simon melting relation [33]. Later measurements were extended to 15 GPa and 526 K [5]; the resulting data were fit to the analytical Kechin melting model [34], which suggested a melting temperature maximum at higher pressure. With increasing pressure, higher temperatures and smaller samples are required, thereby making reliable melting measurements at high *P*-*T* conditions technically challenging. For example, static compression experiments have been

carried out at higher *P-T* conditions (*e.g.,* ~250 GPa and 480 K), but the melting line was not identified [35]. Reported melting data at megabar pressures using laser heating DAC techniques have resulted in large error bars and are not fully consistent [7, 8, 36, 37] as a result of potentially large, non-uniform temperature distributions and the variable absorption-dependent stability for the heating temperature. Furthermore, possible chemical reactions between hydrogen and the absorber, which is needed to couple with the laser, can complicate the observations. The situation becomes more acute at multimegabar pressure, owing in part to the very small dimensions of the absorber in the small sample chamber. Accurate identification of melting at higher pressures can also be a problem. Discontinuous changes of intramolecular vibration frequencies (vibrons), have also been used as a melting criterion at lower pressures [6] but these shifts become weak and undetectable at pressures above ~50 GPa.

To overcome the experimental issues described above, we developed techniques with improved heating and more precise melting discrimination at high *P-T* conditions. This improved technique allows the study of hydrogen in the DAC up to 300 GPa at 295 - 1000 K [38]. Raman spectroscopy has been combined with this heating technique for *in situ* high *P-T* measurements. Several methods were used to identify the melting transitions. The white light interference pattern created between the two opposing diamond anvils was monitored together with visual observation; this is an effective method for detecting the melting point to just above 100 GPa. With this technique [39] the interference pattern, which typically shifts monotonically with temperature, can exhibit a sudden shift when there is a change in refractive index between phases such as solid and fluid. In addition, motion of small debris within the sample (*e.g*., from the gasket upon pressure-induced deformation or fine powder of the optical pressure sensor), is often observed concomitantly with abrupt changes in the interference pattern. Taken together, both provide strong evidence that the transition is to a high-temperature diffusive state (*i.e.*, melting). The interference method cannot be used when the refractive index of diamond and hydrogen approaches each other around 140 GPa as the contrast of the interference pattern disappears under these conditions. Moreover, at higher pressures, sample sizes can be too small to observe any debris motion in the sample chamber. In this situation, the disappearance of the Raman-active lattice modes becomes the most reliable diagnostic of melting of the solid.

We conducted more than 10 heating runs at pressures of 140 to 300 GPa with freshly loaded samples for each run. Among these, 6 runs reached the melting point (Fig. 1). Although the measured data show general agreement with the predicted trends, the melting temperatures are lower than those predicted by several theoretical calculations near the maximum. In addition, predicted melting temperatures from several calculations are significantly lower than the measured data at the highest pressures. Figure 2 shows changes in the low-frequency lattice modes and high-frequency vibrons with increasing temperature at different pressures. Previous experiments have shown that near ~220 GPa at 300 K solid hydrogen transforms from the hcp structure of phase I to 'ionic' phase III and then the layered phase IV structure [40-45]. The low-frequency Raman spectra above 140 GPa and 300 K [see Fig. 2(a)] consist of broadened rotons (L_2) and the optical phonon (L_3) derived from the E_{2g} mode of phase I [46]. These spectral features were found to persist up to ~225 GPa at 300 K consistent with previous work [44]. At the transition, a sharp band appears in the Raman spectrum at ~300 cm^{-1} [L_1 in Fig. 2(b-d)]. This peak is assigned to the libron mode related to the graphene-like layer of phase IV [47]. This sharp peak is the strongest low-frequency feature to above 300 GPa at 300 K. The intensity of the phonon increased abruptly at 250 GPa and 300 K accompanied by an increase in pressure dependence of its frequency [44]. The higher frequency spectrum at 300 K has two vibron peaks: a strong ν_1 peak assigned to strongly coupled H_2 in the graphene-like layer, and a second vibron (ν_2) at higher frequency [Fig. 2(f-h)] assigned to weakly coupled molecular H_2 in the Br-like layer of phase IV [42, 43, 47]. Notably, a vibron is observed in all heating runs even when the crystal has apparently melted. At room temperature, the ν_2 vibron derived from phase IV can be observed up to the highest pressure studied here. However, the peak disappeared upon heating at different pressures. Furthermore, a new peak emerged at 2700 cm^{-1} when the sample is heated to above 373 K at 300 GPa [Fig. 2(h)].

The changes in spectra with temperature are interpreted as arising from multiple phase transitions of the solid. Several trends can be identified from careful examination of the Raman spectra. As shown in the top panel of Fig. 2, the intensities of all the Raman modes decrease on heating; the lattice modes eventually disappear at a critical temperature, which we identify as the melting point at a given pressure. This is reliable and robust evidence for the melting transition. A vibron feature is always observed, regardless of the pressure and temperature in the runs where

we identify melting; this observation indicates that the disappearance of the low-frequency lattice modes is not due to the loss of the sample. The disappearance of the lowest frequency libron peak (L_1) correlates with the behavior of the ν_2 vibron, with both vanishing at lower temperature than the other modes although not necessarily at same temperature and pressure. The disappearance of the ν_2 vibron is evidence for a transition to another phase, including possible dissociations of the H_2 molecules. According to simulations [48], the hydrogen molecules in the graphenic layers of phase IV are more weakly bound, and exhibit significant intermolecular atomic exchange. The extent to which additional H_2 molecules are fully dissociated in that phase (or phases) before melting remains to be determined.

Figure 3 compares the melting line determined in this study with other experimental data as well as theoretical calculations for the fluid. Below ~140 GPa, the profile of the melting line is similar to previous experimental studies, though the maximum temperature of melting is lower. The maximum is located at 70 ± 3 GPa and 826 ± 10 K based on a Kechin equation fit to 140 GPa, above which the slope of the melting line changes This pressure is close to where weak discontinuous pressure-induced shifts in the vibron have been observed near 300 K that suggested a weak structural transition in phase I (*i.e.,* to phase I') [17, 18]. A transition in phase I at high temperature was also predicted in early theoretical calculations [19, 20]. Indeed, the present measurements show a change in temperature dependence of the vibron frequency at lower temperatures consistent with the proposed I-I' transition extending into the *P-T* range explored here [38].

Noticeable discontinuities in the pressure dependence of the ν_1 frequency and peak width prior to melting were observed at ~140 GPa, with additional changes near 230 GPa (Fig. S5) [38]. The spectral changes suggest a change in local structure around H_2 molecules and/or a structural phase transition. These pressures are close to the low-temperature extension of predicted fluid-fluid transition lines [12], though more recent calculations shift the predicted transitions to still higher pressures [32]. The continuity of the vibron in passing from solid to liquid (Fig. S6) [38] reveals that the degree of molecular association-dissociation is similar to that of the solid above the melting line. The results are consistent with the lack of a significant density change across melting, which in turn is implied by the relatively flat slope of melting curve in this pressure range. The discontinuous changes in the vibron frequencies indicate two first-order pressure-

induced structural transitions in the solid at these conditions. It is possible that these first-order transitions are related to the predicted fluid-fluid transitions [10, 12, 27, 28, 30-32]. Additional compression experiments at high temperature in the stability of the liquid are needed to test this hypothesis. As mentioned above, such measurements are challenging in view of the general difficulty in containing the molten hydrogen with diamond anvils under these conditions in static compression experiments. Further, the Raman measurements show a significant further increase in the width of the vibron above ~230 GPa at 630 K below the melting line (Fig. S5) [38]. The width of the ν_1 vibron peak at 300 K in phase IV has been attributed to proton dynamics associated with short-lived molecular species in the graphene-like layer of the structure, as mentioned above [48]. It is tempting to associate the peak broadening to a further enhancement of molecular dissociation. Explicit calculations of a *P*-*T* dependence of this change, and its relation to changes in the fluid are in progress [49].

A new Raman peak is observed near ~2700 cm^{-1} at 300 GPa and $T > 373$ K (Fig. 2h). The same peak initially was also observed in the heating run at 280 GPa. The appearance of the peak is interpreted as evidence for a new phase. The observation of the new Raman band below the melting temperature and the higher frequency vibron (*e.g.,* ν_1 of phase IV or a related structure) persists to higher *P*-*T* conditions suggests that the sample may be mixed phase at these conditions. The frequency of this vibrational mode suggests a weaker H-H covalent bond and therefore a larger H-H distance. To explain the origin of this peak, Raman spectra for energetically competitive structures proposed previously near 300 GPa were calculated. Agreement between theory and experiment was found for the *Cmca*-4 structure, which is predicted to be metallic and have a strong Raman band at 2730 cm^{-1} together with a very weak lattice mode. Notably, a transition to this structure was invoked to explain the onset of electrical conductivity observed at comparable pressures (270 GPa) [40]. More recently, evidence for a transition to a strongly reflecting phase of solid hydrogen at low temperatures and reportedly higher pressures was published (*i.e.*, a different *P*-*T* domain) [50], but the lack of well-defined spectra, the use of coated diamonds, and uncertainty in the pressure estimation have raised questions about the results and interpretation [51].

Our evidence for a high-temperature metallic phase near 300 GPa may be relevant to the interpretation of recent ramp compression experiments that indicate an abrupt transition to a

strongly reflecting state at comparable pressures [23]. In those experiments, the temperature was not measured and could plausibly overlap the temperatures explored in the present study. If so, our results may help to resolve that discrepancy among dynamic compression studies. As such, the present study bridges the important but less well explored intermediate regime between warm dense fluid and the solid phases at high *P-T* conditions. Taken together with previous work, the results suggest the existence of multiple transitions to different metallic (including semi-metallic and strongly metallic) phases in the solid and fluid at the conditions explored so far in current static and dynamic compression experiments.

Acknowledgments

We are grateful to T. S. Duffy, J. M. McMahon, I. I. Naumov, and G. D. Cody for useful discussions. This work was supported by the Department of Energy (DOE)/National Nuclear Security Administration, through the Carnegie/Department of Energy Alliance Center (CDAC; grant No. DE-NA-0002006), and by DOE Office of Science, Basic Energy Sciences through EFree, an Energy Frontier Research Center (DE-SC0001057).

References

[1] E. Wigner and H. B. Huntington, J. Chem. Phys. **3**, 764 (1935).
[2] N. W. Ashcroft, Phys. Rev. Lett. **21**, 1748 (1968).
[3] H. K. Mao and R. J. Hemley, Rev. Mod. Phys. **66**, 671 (1994).
[4] J. M. McMahon, M. A. Morales, C. Pierleoni, and D. M. Ceperley, Rev. Mod. Phys. **84**, 1607 (2012).
[5] F. Datchi, P. Loubeyre, and R. LeToullec, Phys. Rev. B **61**, 6535 (2000).
[6] E. Gregoryanz, A. F. Goncharov, K. Matsuishi, H. Mao, and R. J. Hemley, Phys. Rev. Lett. **90** (2003).
[7] S. Deemyad and I. F. Silvera, Phys. Rev. Lett. **100**, 155701 (2008).
[8] M. I. Eremets and I. A. Trojan, JETP Letters **89**, 174 (2009).
[9] N. Subramanian, A. F. Goncharov, V. V. Struzhkin, M. Somayazulu, and R. J. Hemley, Proc. Nat. Acad. Sci. U.S.A. **108**, 6014 (2011).
[10] S. A. Bonev, E. Schwegler, T. Ogitsu, and G. Galli, Nature **431**, 669 (2004).
[11] S. M. Davis, A. B. Belonoshko, B. Johansson, N. V. Skorodumova, and A. C. T. van Duin, J. Chem. Phys. **129**, 194508 (2008).
[12] M. A. Morales, C. Pierleoni, E. Schwegler, and D. M. Ceperley, Proc. Natl. Acad. Sci. USA **107**, 12799 (2010).
[13] L. Caillabet, S. Mazevet, and P. Loubeyre, Phys. Rev. B **83**, 094101 (2011).
[14] A. B. Belonoshko, M. Ramzan, H. K. Mao, and R. Ahuja, Sci. Report. **3**, 2340 (2013).
[15] H. Y. Liu, E. R. Hernandez, J. Yan, and Y. M. Ma, J. Phys. Chem. **117**, 11873 (2013).
[16] E. Babaev, A. Sudbo, and N. W. Ashcroft, Nature **431**, 666 (2004).
[17] A. F. Goncharov, I. I. Mazin, J. H. Eggert, R. J. Hemley, and H. K. Mao, Phys. Rev. Lett. **75**, 2514 (1995).
[18] B. J. Baer, W. J. Evans, and C. S. Yoo, Phys. Rev. Lett. **98**, 235503 (2007).
[19] M. P. Surh, K. J. Runge, T. W. Barbee, E. L. Pollock, and C. Mailhiot, Phys. Rev. B **55**, 11330 (1997).
[20] T. Cui, Y. Takada, Q. Cui, Y. Ma, and G. Zou, Phys. Rev. B **64**, 024108 (2001).
[21] W. J. Nellis, S. T. Weir, and A. C. Mitchell, Phys. Rev. B **59**, 3434 (1999).
[22] V. E. Fortov, R. I. Ilkaev, V. A. Arinin, V. V. Burtzev, V. A. Golubev, I. L. Iosilevskiy, V. V. Khrustalev, A. L. Mikhailov, M. A. Mochalov, V. Y. Ternovoi, and M. V. Zhernokletov, Phys. Rev. Lett. **99**, 185001 (2007).
[23] M. D. Knudson, M. P. Desjarlais, A. Becker, R. W. Lemke, K. R. Cochrane, M. E. Savage, D. E. Bliss, T. R. Mattsson, and R. Redmer, Science **348**, 1455 (2015).
[24] V. Dzyabura, M. Zaghoo, and I. F. Silvera, Proc. Natl. Acad. Sci. USA **110**, 8040 (2013).
[25] R. S. McWilliams, D. A. Dalton, M. F. Mahmood, and A. F. Goncharov, Phys. Rev. Lett. **116** (2016).
[26] M. Zaghoo, A. Salamat, and I. F. Silvera, Phys. Rev. B **93**, 155128 (2016).
[27] S. Scandolo, Proc. Natl. Acad. Sci. USA **100**, 3051 (2003).
[28] W. Lorenzen, B. Holst, and R. Redmer, Phys. Rev. B **82**, 195107 (2010).
[29] I. Tamblyn and S. A. Bonev, Phys Rev Lett **104**, 065702 (2010).
[30] G. Mazzola, S. Yunoki, and S. Sorella, Nature Commun. **5**, 3487 (2014).
[31] G. Mazzola and S. Sorella, Phys. Rev. Lett. **114**, 105701 (2015).
[32] C. Pierleoni, M. A. Morales, G. Rillo, M. Holzmann, and D. M. Ceperley, Proc. Natl. Acad. Sci. USA **113**, 4953 (2016).

[33] V. Diatschenko, C. W. Chu, D. H. Liebenberg, D. A. Young, M. Ross, and R. L. Mills, Phys. Rev. B **32**, 381 (1985).
[34] V. V. Kechin, Phys. Rev. B **65**, 052102 (2001).
[35] R. T. Howie, P. Dalladay-Simpson, and E. Gregoryanz, Nature Mat. **14**, 495 (2015).
[36] N. Subramanian, A. F. Goncharov, V. V. Struzhkin, M. Somayazulu, and R. J. Hemley, Proc. Natl. Acad. Sci. USA **108**, 6014 (2011).
[37] A. F. Goncharov, R. J. Hemley, and E. Gregoryanz, Phys. Rev. Lett. **102**, 149601 (2009).
[38] See Supplemental Materials for further details concerning the experiments and calculations, including Refs. [5, 41, 44, 52-57].
[39] C. S. Zha, R. J. Hemley, S. A. Gramsch, H. K. Mao, and W. A. Bassett, J. Chem. Phys. **126** (2007).
[40] M. I. Eremets and I. A. Troyan, Nature Mat. **10**, 927 (2011).
[41] R. T. Howie, C. L. Guillaume, T. Scheler, A. F. Goncharov, and E. Gregoryanz, Phys. Rev. Lett. **108**, 125501 (2012).
[42] H. Liu, L. Zhu, W. Cui, and Y. Ma, J. Chem. Phys. **137**, 074501 (2012).
[43] C. J. Pickard and M. Martinez-Canales, Phys. Rev. B **85**, 214114 (2012).
[44] C. S. Zha, R. E. Cohen, H. K. Mao, and R. J. Hemley, Proc. Natl. Acad. Sci. USA **111**, 4792 (2014).
[45] C.-S. Zha, Z. Liu, M. Ahart, R. Boehler, and R. J. Hemley, Phys. Rev. Lett. **110**, 217402 (2013).
[46] R. J. Hemley, H. K. Mao, and J. F. Shu, Phys. Rev. Lett. **65**, 2670 (1990).
[47] A. F. Goncharov, J. S. Tse, H. Wang, J. Yang, V. V. Struzhkin, R. T. Howie, and E. Gregoryanz, Phys. Rev. B **87**, 024101 (2013).
[48] H. Liu and Y. Ma, Phys. Rev. Lett. **110**, 025903 (2013).
[49] H. Liu, to be published.
[50] R. P. Dias and I. F. Silvera, Science **355**, 715 (2017).
[51] See *e.g.*, M.I. Eremets and A. P. Drozdov, arXiv:1702.05125; P. Loubeyre, F. Occelli, and P. Dumas, arXiv:1702.07192.
[52] Y. Akahama and H. Kawamura, J. App. Phys. **96**, 3748 (2004).
[53] F. Datchi, A. Dewale, P. Loubeyre, R. Letoullec, Y. Le Godec, and B. Canny, High Press. Res. **27**, 447 (2007).
[54] A. Fonari and S. Stauffer, https://github.com/raman-sc/VASP (2013).
[55] R. S. Hixson and N. Fritz, J. Appl. Phys. **71**, 1721 (1992).
[56] D. Porezag and M. R. Pederson, Phys. Rev. B **54**, 7830 (1996).
[57] C. S. Zha and W. A. Bassett, Rev. Sci. Instrum. **74**, 1255 (2003).

Figure Captions

Figure 1. Pressure-temperature paths for different heating runs. The small pressure variations were recorded by diamond Raman spectra collected at each temperature increments (see text). Solid and open symbols indicate *P-T* regions where solid and melt, respectively, were observed; pink dashed line, Bonev et al. [10]; blue dashed line, Morales et al. [12]; red dotted line, Caillabet et al. [13]; green dotted-dash line, Belonoshko et al. [14]; red dashed line, Liu et al. [15]. The inset shows examples of diamond anvil Raman spectra for measurement of pressure during heating.

Figure 2. Selected Raman spectra of hydrogen at selected temperatures and pressures. *Top*: Low-frequency region. The flattened spectra (red thick dashed lines) show the disappearance of lattice modes on melting. The black thin dashed lines show the behavior of individual modes during heating. *Bottom:* High-frequency vibron region. Spectra in red thick dashed lines are those obtained at melting; the labels ν_1 and ν_2 represent the vibrons from the two-layer structure of phase IV. The asterisk indicates the new peak that appears above ~280 GPa on heating.

Figure 3. Hydrogen *P-T* phase diagram. The data below 140 GPa have been fit with a Kechin equation: $T_m(K) = 14.025(1 + P/a)^b \exp(-P/c)$ with $a = 0.029683$, $b = 0.60224$, $c = 116.4$. Red solid circles and black solid lines are the melting points and the fitted melting lines from this study. The two black dashed lines at ~140 and ~230 GPa represent proposed phase lines in the solid. Previous experimental data: downwards open triangles, Diatchenko et al. [33], crosses Datchi et al. [5]; open squares, Gregoryanz et al. [6]; diamond, Deemyad et al. [7]; upwards open triangles, Eremets et al. [8]; open circles, Subramanian et al. [36]; solid upwards triangles (150 GPa, absorption onset; 300 GPa, reflectivity onset), Knudson et al. [23]; solid downwards triangle Zaghoo et al. [26]. Previous proposed phase lines: red solid line, Zha et al.[45]; light gray short dashed lines, Howie et al. [35]; blue dotted line, Bonev et al. [10]; red dotted line, Caillabet et al. [13]; gray long dashed line and green dashed lines, Morales et al. [12]; red dashed line, Lorenzen et al. [28]; pink short dash line, Pierleoni et al. [32]; green dotted dash line, Belonosko et al. [14].

Figures

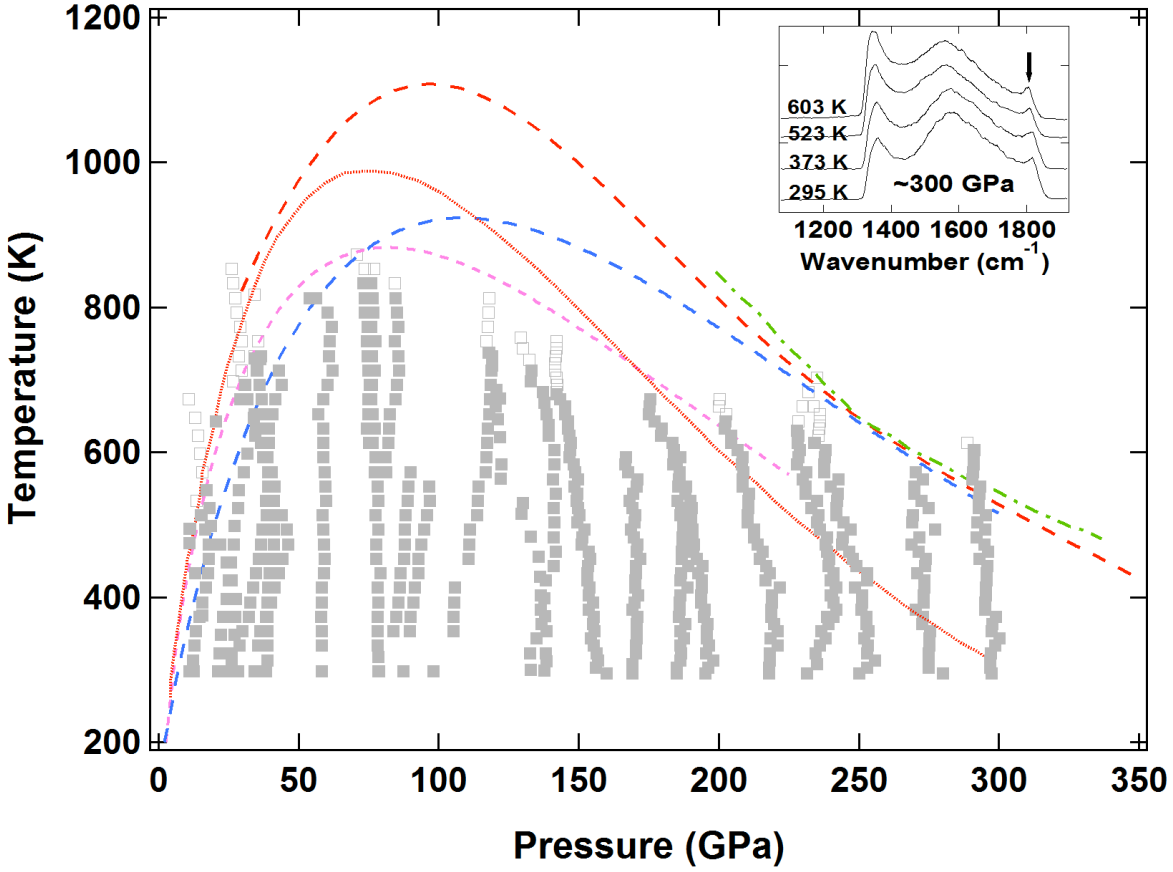

Figure 1

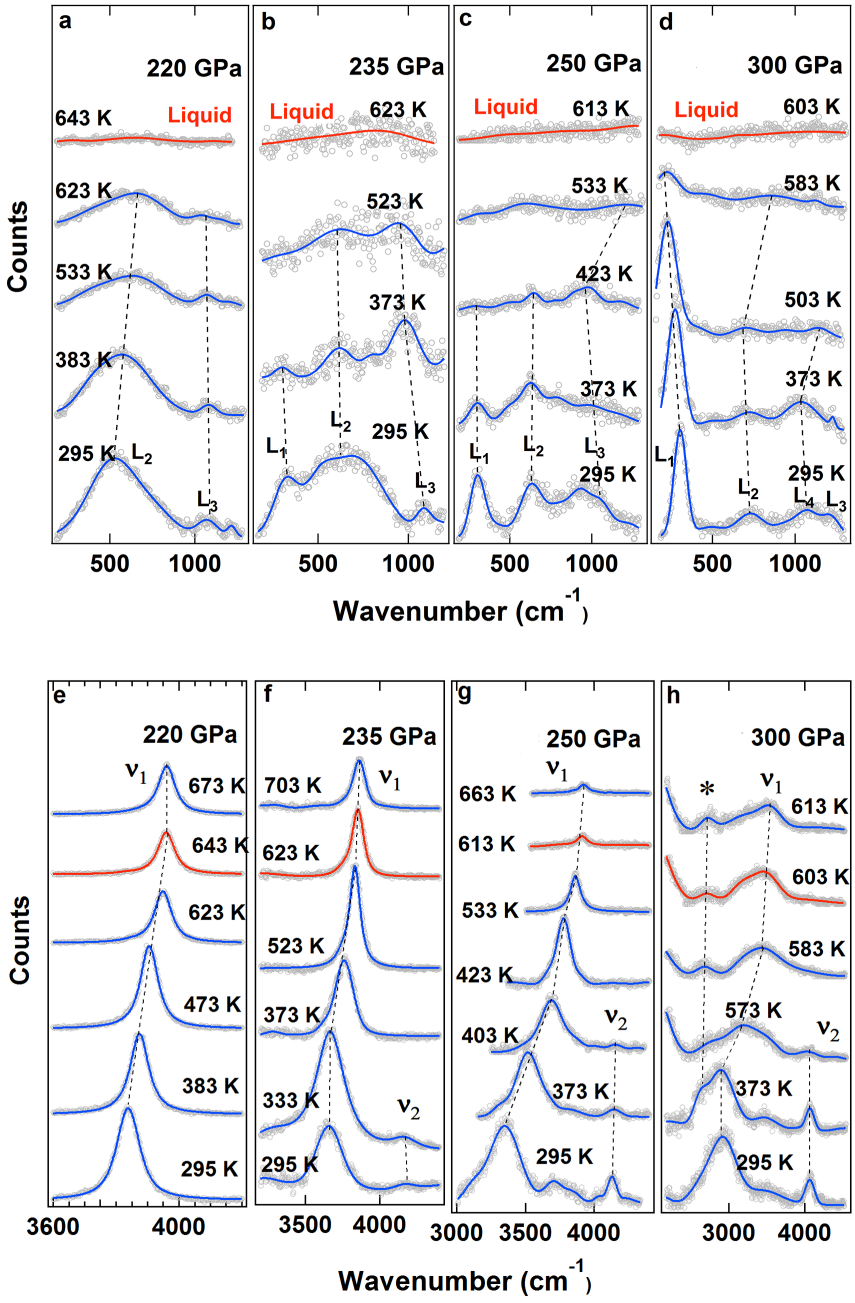
a
220 GPa
643 K
Liquid
623 K
533 K
383 K
295 K
L2
L3
b
235 GPa
Liquid
623 K
523 K
373 K
L2
295 K
L1
L3
c
250 GPa
Liquid
613 K
533 K
423 K
373 K
L1
L2
L3
295 K
d
300 GPa
Liquid
603 K
583 K
503 K
373 K
L1
L2
L4
L3
295 K
Counts
500
1000
Wavenumber (cm-1)
e
220 GPa
ν1
673 K
643 K
623 K
473 K
383 K
295 K
f
235 GPa
703 K
ν1
623 K
523 K
373 K
333 K
ν2
295 K
g
250 GPa
663 K
ν1
613 K
533 K
423 K
403 K
ν2
373 K
295 K
h
300 GPa
*
ν1
613 K
603 K
583 K
573 K
ν2
373 K
295 K
Counts
3600
4000
3500
3000
Wavenumber (cm-1)

Figure 2

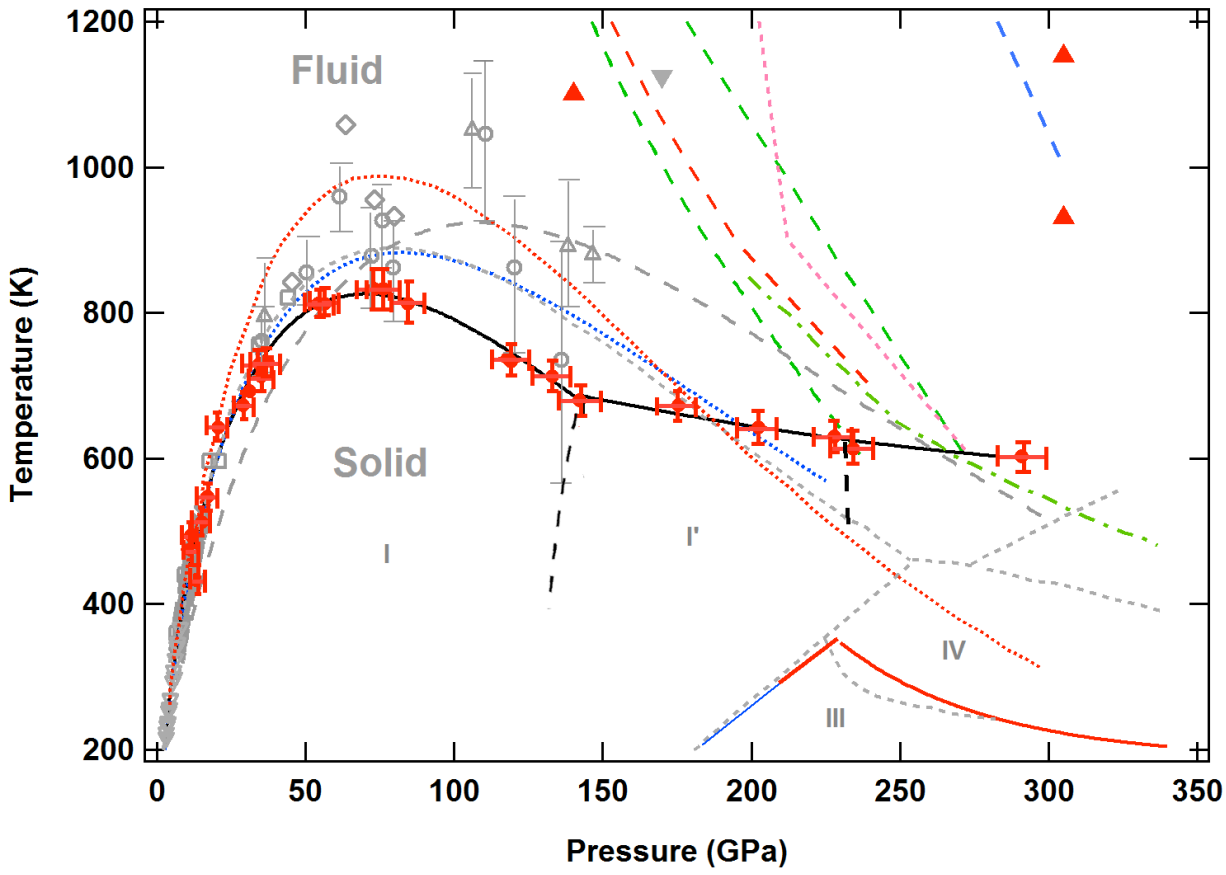
Fluid
Solid
I
I'
III
IV
Temperature (K)
Pressure (GPa)
1200
1000
800
600
400
200
0
50
100
150
200
250
300
350

Figure 3